

Effects of a chiral three-nucleon force on nucleus-nucleus scattering

Kosho Minomo,^{1,*} Masakazu Toyokawa,² Michio Kohno,^{3,1} and Masanobu Yahiro²

¹Research Center for Nuclear Physics, Osaka University, Ibaraki 567-0047, Japan

²Department of Physics, Kyushu University, Fukuoka 812-8581, Japan

³Physics Division, Kyushu Dental University, Kitakyushu 803-8580, Japan

(Dated: April 23, 2014)

We investigate the effects of chiral NNLO three-nucleon force (3NF) on nucleus-nucleus elastic scattering, using a standard prescription based on the Brueckner-Hartree-Fock method and the g -matrix folding model. The g -matrix calculated in nuclear matter from the chiral N^3 LO two-nucleon forces (2NF) is close to that from the Bonn-B 2NF. Because the Melbourne group have already developed a practical g -matrix interaction by localizing the nonlocal g -matrix calculated from the Bonn-B 2NF, we consider the effects of chiral 3NF, in this first attempt to study the 3NF effects, by modifying the local Melbourne g -matrix according to the difference between the g -matrices of the chiral 2NF and 2NF+3NF. For nucleus-nucleus elastic scattering, the 3NF corrections make the folding potential less attractive and more absorptive. The latter novel effect is due to the enhanced tensor correlations in triplet channels. These changes reduce the differential cross section at the middle and large angles, improving the agreement with the experimental data for ^{16}O - ^{16}O scattering at 70 MeV/nucleon and ^{12}C - ^{12}C scattering at 85 MeV/nucleon.

PACS numbers: 21.30.Fe, 24.10.Ht, 25.70.Bc

Introduction. How important are three-nucleon forces (3NFs) in nuclear physics? This is one of the most important issues. This long-standing subject started with the 2π -exchange 3NF proposed by Fujita and Miyazawa [1]. For light nuclei, attractive 3NFs were introduced to reproduce the binding energies [2]. In symmetric nuclear matter, meanwhile, repulsive 3NFs were introduced to explain empirical saturation properties; for example see Refs. [3–6].

It is quite hard to determine 2NF and 3NF phenomenologically. This problem can be solved by chiral effective field theory (Ch-EFT) [7–10], since the theory systematically organizes interactions among nucleons. The roles of chiral 3NF was recently analyzed in light nuclei [11–14]. For symmetric nuclear matter, the g -matrix calculated from chiral N^3 LO 2NF plus NNLO 3NF [7, 9] well explain the empirical saturation properties with no adjustable parameter [15–18]. Scattering and reaction phenomena are important processes to explore 3NF effects.

Microscopic understanding of nucleon-nucleus and nucleus-nucleus scattering is another important subject in nuclear physics. The standard method of describing the scattering is the g -matrix folding model [19–24] with the local-density approximation. In the framework, the 3NF effects appear through the density dependence of the g -matrix. The CEG07 g -matrix is constructed from the 2NF based on the extended soft core model [25, 26] and 3NF effects are empirically taken into account by introducing the density-dependent vector-meson mass that reproduces empirical saturation properties of symmetric nuclear matter [27–29]. In the g -matrix calculation of Ref. [30], meanwhile, phenomenological 3NFs such as Urbana IX [31] and the three-nucleon interaction model [32, 33] are added to AV18 2NF [34]. Since these phenomenological 3NFs are also introduced to

reproduce saturation properties of symmetric nuclear matter, they make the g -matrix less attractive and less absorptive at densities (ρ) higher than the normal density ρ_0 . The 3NF effects then reduce the folding potential $U(R)$ particularly at small distances (R). For nucleus-nucleus elastic scattering, the 3NF effects are remarkable particularly at the middle and large angles where projectile and target densities are largely overlapped, although the strength of the imaginary part of $U(R)$ is adjusted to reproduce the experimental data in the analyses [29]. The question to be addressed now is how the effects of chiral 3NF appear in nucleus-nucleus elastic scattering.

In this Rapid Communication, we investigate the effects of chiral NNLO 3NF on nucleus-nucleus scattering, using the Brueckner-Hartree-Fock (BHF) method for nuclear matter and the g -matrix folding model for the scattering. In the nuclear matter calculations, furthermore, 3NFs are treated with the mean field approximation [32, 35–37], i.e., by averaging 3NFs over the third nucleon in the Fermi sea, since it is quite hard to treat three-body correlations in nuclear matter. This approximation is considered to be good for the low transferred-momentum components of the g -matrix. We then present the following simple prescription, as the first estimate of chiral-3NF effects on nucleus-nucleus scattering.

For nuclear matter, the single-particle potential \mathcal{U} is determined from the diagonal component of the g -matrix. The \mathcal{U} calculated from chiral 2NF is close to that from Bonn-B 2NF [38]. Hence, the effects of chiral 3NF can be expressed with the ratio of the \mathcal{U} calculated from chiral 2NF+3NF to that from Bonn-B 2NF. For finite nuclei, the Melbourne group already presents a practical g -matrix interaction by localizing the nonlocal g -matrix calculated from Bonn-B 2NF [23]. The Melbourne g -matrix is highly reliable for nucleon-nucleus scattering where the 3NF effects are considered to be small [30], since the folding potential with the Melbourne g -matrix well reproduces the experimental data with no adjustable parameter [23, 39, 40]. The effects of chiral 3NF

*minomo@rcnp.osaka-u.ac.jp

are then introduced to the local Melbourne g -matrix by multiplying it by the ratio. With the simple prescription, we make a qualitative discussion about the effects of chiral 3NF on nucleus-nucleus scattering. We consider ^{16}O - ^{16}O scattering at 70 MeV/nucleon and ^{12}C - ^{12}C scattering at 85 MeV/nucleon, since chiral EFT is good at lower incident energies (E).

We first investigate the effects of chiral NNLO 3NF on symmetric nuclear matter through the \mathcal{U} that corresponds to the folding potential $U(R)$ in nucleus-nucleus elastic scattering, and calculate $U(R)$ from the Melbourne interaction with chiral-3NF corrections to analyze the effects on nucleus-nucleus scattering.

BHF calculations. Following Ref. [18], we evaluate the single-particle potential with the BHF method for positive energy E from chiral N^3LO 2NF plus NNLO 3NF with the cut-off energy $\Lambda = 550$ MeV [7, 9]. Here the chiral NNLO 3NF V_{123} is reduced to an effective 2NF $V_{12(3)}$ with the mean-field approximation, that is, by integrating the 3NF over the third nucleon, and nuclear matter calculations are done from the combination of N^3LO 2NF V_{12} and $V_{12(3)}$ in the standard manner.

The single-particle potential $\mathcal{U}^{ST}(k_F, E)$ thus obtained depends on E , total spin (S) and total isospin (T) of two nucleons and the Fermi momentum $\hbar k_F$. The potential is related to the g -matrix G^{ST} as

$$\mathcal{U}^{ST}(k_F, E) = \sum_{\mathbf{k}'}^{k_F} \langle \mathbf{k}\mathbf{k}' | G^{ST} + \frac{1}{6} V_{12(3)}^{ST} (1 + \frac{Q}{E - H} G^{ST}) | \mathbf{k}\mathbf{k}' \rangle_A, \quad (1)$$

where $\hbar\mathbf{k}$ and $\hbar\mathbf{k}'$ are momenta of correlated two nucleons, the subscript $| \rangle_A$ means the antisymmetrization between the correlated nucleons, and $Q/(E - H)$ is the nucleon propagator including the Pauli exclusion operator Q ; see Ref. [18] for detail. The momentum $\hbar\mathbf{k}$ is related to E as $E = (\hbar\mathbf{k})^2/(2m) + \text{Re } \mathcal{U}$ for the nucleon mass m . The potential \mathcal{U}^{ST} is mainly determined from the first term G^{ST} on the right hand side of Eq. (1). For example at the normal density, the contribution of the first term is ten times as large as that of the second term having $V_{12(3)}$. In the first term, only the central part of the on-shell component of G^{ST} contributes to the \mathcal{U}^{ST} , but the tensor part of V_{12} and $V_{12(3)}$ affects the central part significantly. The mean-field approximation taken is good for the \mathcal{U}^{ST} that is mainly determined from the on-shell component of G^{ST} .

Results of BHF calculations. Figure 1 displays k_F dependence of $\mathcal{U}^{ST}(k_F, E)$ at $E = 70$ MeV for each S - T channel. The results of chiral 2NF (squares) are close to those of Bonn-B 2NF (triangles) for all the channels except the ^3O channel. For the real part of \mathcal{U}^{ST} in the ^3O channel, the difference between the two results is not small particularly at high densities, but it little affects angular distributions of elastic cross sections, since the magnitude itself is small there.

Comparing the results of chiral 2NF+3NF (circles) with those of chiral 2NF (squares), one can see appreciable changes for the real part of \mathcal{U}^{ST} in the ^1E channel and for the real and imaginary parts in the triplet channels (^3E and ^3O). Chiral

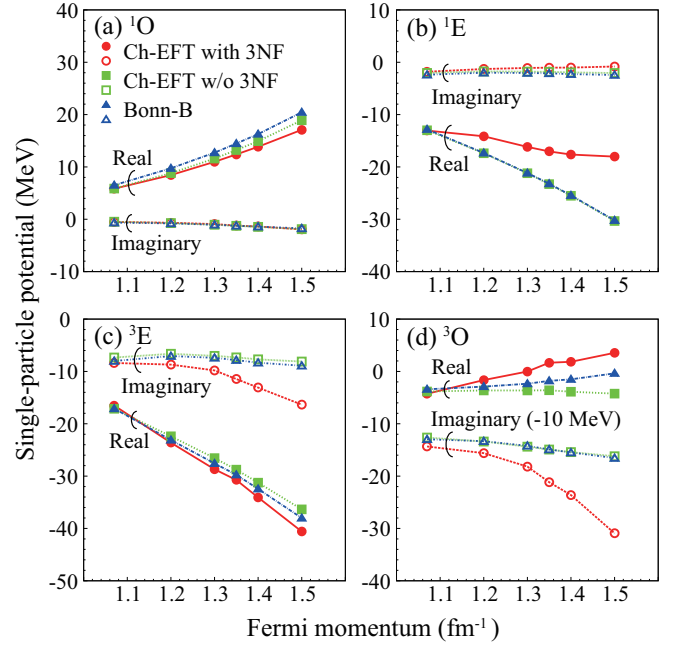


FIG. 1: (Color online) k_F dependence of the single-particle potentials at $E = 70$ MeV for (a) ^1O , (b) ^1E , (c) ^3E , and (d) ^3O channels. The circles, squares, and triangles stand for the results of chiral 2NF+3NF, chiral 2NF and Bonn-B 2NF, respectively. The closed (open) symbols correspond to the real (imaginary) part of the single-particle potentials. For ^3O , the imaginary part is shifted down by 10 MeV.

3NF thus makes \mathcal{U}^{ST} much less attractive for ^1E . This effect has been known to be caused by the suppression of transitions to Δ resonance due to Pauli blocking. For the triplet channels, the 3NF enhances tensor correlations, and thereby makes \mathcal{U}^{ST} much more attractive and absorptive for ^3E and more absorptive but less attractive for ^3O . As the net effect of all the channels, the \mathcal{U}^{ST} becomes much more absorptive because of tensor correlations enhanced by chiral 3NF, and becomes less attractive because of the suppression of transitions to Δ resonance in ^1E . The enhancement of tensor correlations due to chiral 3NF is thus essential in addition to the repulsive nature of chiral 3NF itself. In the region $k_F \lesssim 1.1 \text{ fm}^{-1}$ corresponding to $\rho \lesssim \rho_0/2$, chiral 3NF yields little effect. Such 3NF effects on the \mathcal{U}^{ST} directly reflect nucleus-nucleus scattering through the folding potential $U(R)$, as shown latter. This is natural, because \mathcal{U}^{ST} in nuclear matter plays the same role as $U(R)$ in nucleus-nucleus scattering.

The Melbourne group constructed the local g -matrix interaction $g^{ST}(s; k_F, E)$ from Bonn-B 2NF and showed that the interaction is quite practical and reliable for nucleon-nucleus scattering [23], where s is the coordinate between correlated nucleons. We then introduce 3NF corrections to $g^{ST}(s; k_F, E)$ in the following manner, since the \mathcal{U}^{ST} calculated from Bonn-B 2NF well simulate the results of chiral N^3LO 2NF:

$$g^{ST}(s; k_F, E) \rightarrow f^{ST}(k_F, E) g^{ST}(s; k_F, E) \quad (2)$$

with the factor $f^{ST}(k_F, E)$ defined by

$$f^{ST}(k_F, E) = \mathcal{U}_{(2NF+3NF)}^{ST}(k_F, E) / \mathcal{U}_{(2NF)}^{ST}(k_F, E), \quad (3)$$

where $\mathcal{U}_{(2NF+3NF)}^{ST}(k_F, E)$ and $\mathcal{U}_{(2NF)}^{ST}(k_F, E)$ stand for the single-particle potentials with and without 3NF, respectively. This prescription mainly takes account of the effects of the on-shell component of chiral 3NF on the local Melbourne g -matrix interaction.

Folding-model calculations. Now we consider nucleus-nucleus scattering with the folding model. In the model, the folding potential $U(R)$ is obtained by folding $g^{ST}(s; k_F, E)$ with projectile and target densities in the standard way [24, 29, 41–43], where the Fermi momentum $\hbar k_F$ is replaced by a local Fermi momentum that is evaluated with the frozen density approximation. That is, k_F is estimated from the sum of projectile and target local densities at the middle point of interacting nucleons. As the projectile and target proton densities, we take the phenomenological ones determined from the electron scattering [44], applying proton finite-size corrections to the densities with the standard manner [45]. The neutron densities are assumed to be the same as the proton ones, which is accurate enough for light nuclei.

Results of folding-model calculations. Figure 2 shows the folding potential $U(R)$ for ^{16}O - ^{16}O elastic scattering at 70 MeV/nucleon. The solid (dashed) curve represents the result with (without) 3NF corrections. The potential is mainly determined from the even-channel (^1E and ^3E) components, since the odd-channel (^1O and ^3O) components are almost canceled after the sum of the direct and exchange parts of $U(R)$. For the real part of $U(R)$, chiral 3NF works as a repulsive force, but it is weak because of the offset between the repulsive contribution in ^1E and the attractive one in ^3E . For the imaginary part, chiral 3NF makes $U(R)$ strongly absorptive, since the contribution works additively between ^3E and ^3O channels.

In the previous works of Refs. [27–30], the phenomenological 3NFs work repulsively and less absorptively. For the real part of $U(R)$, the present result is consistent with the previous ones qualitatively, although the repulsive effect is small in the present work but large in the previous works. For the imaginary part, meanwhile, chiral 3NF enhances the absorption of $U(R)$, in contrast to the opposite effect of phenomenological 3NFs. The difference comes from the fact that chiral 3NF enhances tensor correlations but the phenomenological 3NFs do not.

Figure 3 shows differential cross sections for (a) ^{16}O - ^{16}O elastic scattering at 70 MeV/nucleon and (b) ^{12}C - ^{12}C elastic scattering at 85 MeV/nucleon as a function of scattering angle θ in the center of mass system. The solid (dashed) curve corresponds to the result of Melbourne interaction with (without) chiral-3NF corrections. Chiral 3NF reduces the cross sections in middle and large angles ($\theta > 5^\circ$) and hence improves the agreement with the experimental data [46, 47]. Switching off chiral-3NF effects for either the real or the imaginary part of $U(R)$, we find that the interference between the two effects is important at the middle and large angles.

For the ^{16}O - ^{16}O scattering, the result of chiral 2NF+3NF slightly overestimates the experimental data. If the real part

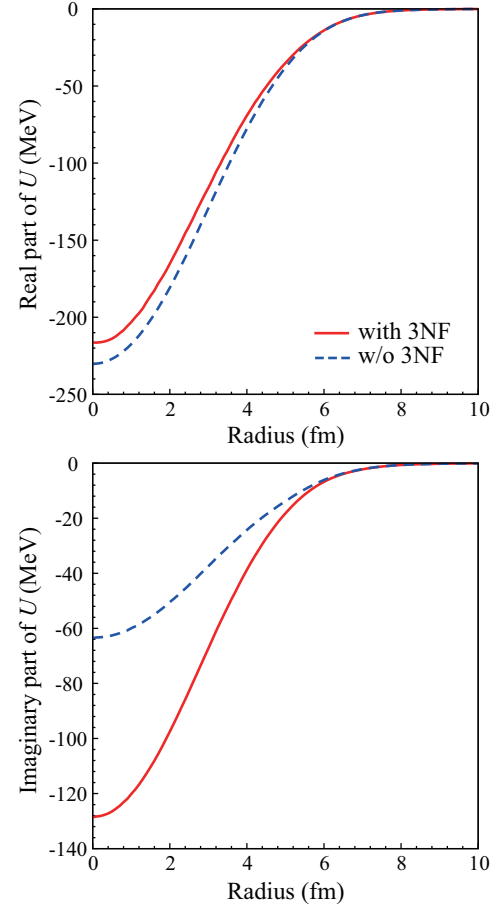


FIG. 2: (Color online) The folding potential for ^{16}O - ^{16}O elastic scattering at 70 MeV/nucleon. The real and imaginary parts of the potential are shown in the upper and lower panels, respectively. The solid (dashed) curve represents the result with (without) 3NF effects.

of the potential is reduced by 10% and the imaginary part is enhanced by 10%, the result can reproduce the data. Since the correction is rather small, as an origin of the difference we can consider higher-order corrections such as off-shell corrections due to chiral 3NF and corrections for the mean-field approximation. For the ^{12}C - ^{12}C scattering, the diffraction pattern is slightly shifted forward in the result of chiral 2NF+3NF compared with the data. The difference may come from projectile and/or target excitations, since the previous work of Ref. [48] shows that the excitation effects slightly shift the diffraction pattern backward. The higher-order corrections mentioned above may be masked by the excitation effects. Further analysis along this line is quite interesting as a future work.

Total reaction cross sections σ_R are mainly determined from the imaginary part of $U(R)$. We then check whether the present potential with 3NF corrections reproduces measured σ_R . Table I shows σ_R for ^{16}O - ^{16}O scattering at 70 MeV/nucleon and ^{12}C - ^{12}C scattering at 85 MeV/nucleon. The experimental data are available for the ^{12}C - ^{12}C scattering, but not for the ^{16}O - ^{16}O scattering. Chiral 3NF enhances σ_R only by a few percent, since the effects appear

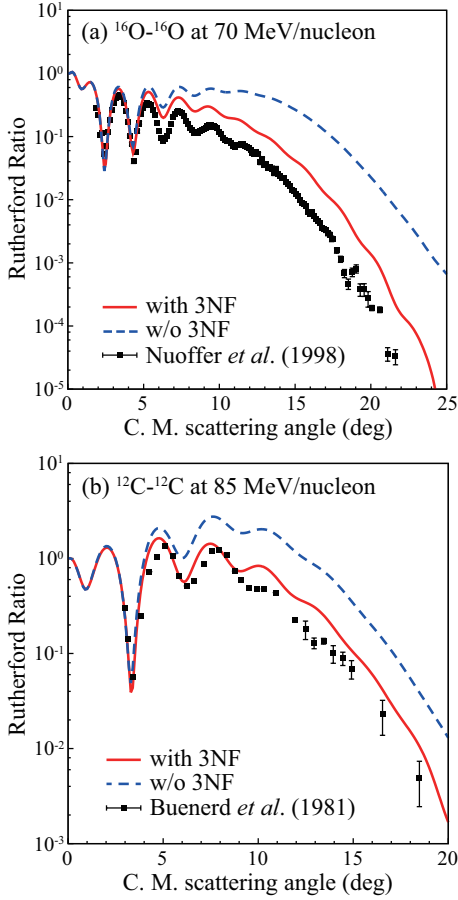


FIG. 3: (Color online) The differential cross sections of (a) ^{16}O - ^{16}O elastic scattering at 70 MeV/nucleon and (b) ^{12}C - ^{12}C elastic scattering at 85 MeV/nucleon as a function of the scattering angle in the center of mass system. The solid (dashed) line corresponds to the result of Melbourne interaction with (without) 3NF corrections. The experimental data are taken from Refs. [46, 47].

only at small R where $U(R)$ already has strong absorption. The calculated result slightly overestimates the experimental data [49], but it is not serious at all. The Melbourne g -matrix interaction with 3NF corrections is thus reliable also for σ_R .

TABLE I: Total reaction cross sections for nucleus-nucleus scattering around 70 MeV/nucleon (in the unit of mb). The experimental data is taken from Ref. [49].

system	with 3NF	w/o 3NF	Exp. [49]
^{16}O - ^{16}O @70MeV/nucleon	1423	1401	—
^{12}C - ^{12}C @85MeV/nucleon	1025	989	998 ± 13

Summary. We have made a qualitative discussion about the

effects of chiral NNLO 3NF on nucleus-nucleus elastic scattering, using the simple prescription of Eqs. (2) and (3). In this prescription, on-shell corrections due to chiral 3NF are introduced to the local Melbourne g -matrix interaction. It is to be stressed that we have not introduced any ad hoc phenomenological adjustment.

For nuclear matter, chiral 3NF makes the single-particle potentials less attractive for the ^1E channel and more absorptive for the triplet channels. The effects mainly comes from the 2π exchange process. For the triplet channels, the diagram enhances tensor correlations and hence the absorption. These 3NF corrections are incorporated in the folding potential for nucleus-nucleus scattering by modifying the local Melbourne g -matrix interaction by the multiplicative factor prescribed as Eqs. (2) and (3). The corrections make the folding potential less attractive and more absorptive. Since the folding potential is mainly determined from the ^1E - and ^3E -channel components, we can conclude that the repulsive correction to the folding potential comes from the suppression of transitions to Δ resonance and the absorptive correction is originated in the enhancement of tensor correlations. The two effects reduce differential elastic cross sections for both ^{16}O - ^{16}O scattering at 70 MeV/nucleon and ^{12}C - ^{12}C scattering at 85 MeV/nucleon. Eventually, chiral 3NF improves the agreement with the experimental data.

It is instructive to note the qualitative difference of the present result from other similar studies in the literature. In the previous works of Refs. [27–30], the phenomenological 3NFs make the folding potential $U(R)$ less attractive and less absorptive. The present result is consistent with the previous ones qualitatively for the real part of $U(R)$, although the repulsive effect is small in the present work but large in the previous works. For the imaginary part, meanwhile, chiral 3NF makes $U(R)$ more absorptive, whereas the phenomenological 3NFs do $U(R)$ less absorptive. The difference comes from the fact that chiral 3NF enhances tensor correlations but the phenomenological 3NFs do not.

The on-shell corrections due to chiral 3NF surely improve the agreement with the experimental data on nucleus-nucleus elastic scattering, but the agreement is not perfect. This may come from higher-order corrections such as off-shell corrections due to chiral 3NF and corrections for the mean-field approximation. Further analysis along this line toward deeper microscopic understanding of nucleus-nucleus scattering is quite interesting as a future work.

Acknowledgements

This work is supported in part by by Grant-in-Aid for Scientific Research (Nos. 244137, 25400266, and 26400278) from Japan Society for the Promotion of Science (JSPS).

-
- [1] J. Fujita and H. Miyazawa, *Prog. Theor. Phys.* **17**, 366 (1957).
 - [2] R. B. Wiringa and S. C. Pieper, *Phys. Rev. Lett.* **89**, 182501 (2002).
 - [3] R. B. Wiringa, V. Fiks, and A. Fabrocini, *Phys. Rev. C* **38**, 1010 (1988).
 - [4] H. Mütter and A. Polls, *Prog. Part. Nucl. Phys.* **45**, 243 (2000).
 - [5] Y. Dewulf, W. H. Dickhoff, D. Van Neck, E. R. Stoddard, and M. Waroquier, *Phys. Rev. Lett.* **90**, 152501 (2003).
 - [6] S. K. Bogner, A. Schwenk, R. J. Furnstahl, and A. Nogga, *Nucl. Phys. A* **763**, 59 (2005).
 - [7] E. Epelbaum, W. Glöckle, and Ulf-G. Meißner, *Nucl. Phys. A* **747**, 362 (2005).
 - [8] E. Epelbaum, H.-W. Hammer, and Ulf-G. Meißner, *Rev. Mod. Phys.* **81**, 1773 (2009).
 - [9] K. Hebeler, S. K. Bogner, R. J. Furnstahl, A. Nogga, and A. Schwenk, *Phys. Rev. C* **83**, 031301(R) (2011).
 - [10] R. Machleidt and D. R. Entem, *Phys. Rep.* **503**, 1 (2011).
 - [11] E. Epelbaum, A. Nogga, W. Glöckle, H. Kamada, Ulf-G. Meißner, and H. Witała, *Phys. Rev. C* **66**, 064001 (2002).
 - [12] A. Nogga, P. Navrátil, B. R. Barrett, and J. P. Vary, *Phys. Rev. C* **73**, 064002 (2006).
 - [13] P. Navrátil, V. G. Gueorguiev, J. P. Vary, W. E. Ormand, and A. Nogga, *Phys. Rev. Lett.* **99**, 042501 (2007).
 - [14] R. Skibiński *et al.*, *Phys. Rev. C* **84**, 054005 (2011).
 - [15] F. Sammarruca, B. Chen, L. Coraggio, N. Itaco, and R. Machleidt, *Phys. Rev. C* **86**, 054317 (2012).
 - [16] M. Kohno, *Phys. Rev. C* **86**, 061301(R) (2012).
 - [17] A. Carbone, A. Polls, and A. Rios, *Phys. Rev. C* **88**, 044302 (2013).
 - [18] M. Kohno, *Phys. Rev. C* **88**, 064005 (2013).
 - [19] J. P. Jeukenne, A. Lejeune and C. Mahaux, *Phys. Rev. C* **16**, 80 (1977).
 - [20] G. Bertsch, J. Borysowicz, H. McManus, and W.G. Love, *Nucl. Phys. A* **284**, 399(1977).
 - [21] F.A. Brieva and J.R. Rook, *Nucl. Phys. A* **291**, 299 (1977); *ibid.* **291**, 317 (1977); *ibid.* **297**, 206 (1978).
 - [22] N. Yamaguchi, S. Nagata and T. Matsuda, *Prog. Theor. Phys.* **70**, 459 (1983); N. Yamaguchi, S. Nagata and J. Michiyama, *Prog. Theor. Phys.* **76**, 1289 (1986).
 - [23] K. Amos, P. J. Dortmans, H. V. von Geramb, S. Karataglidis, and J. Raynal, *Adv. Nucl. Phys.* **25**, 275 (2000).
 - [24] D. T. Khoa and G. R. Satchler, *Nucl. Phys. A* **668**, 3 (2000).
 - [25] Th. A. Rijken, *Phys. Rev. C* **73**, 044007 (2006).
 - [26] Th. A. Rijken and Y. Yamamoto, *Phys. Rev. C* **73**, 044008 (2006).
 - [27] T. Furumoto, Y. Sakuragi, and Y. Yamamoto, *Phys. Rev. C* **78**, 044610 (2008).
 - [28] T. Furumoto, Y. Sakuragi, and Y. Yamamoto, *Phys. Rev. C* **79**, 011601(R) (2009).
 - [29] T. Furumoto, Y. Sakuragi, and Y. Yamamoto, *Phys. Rev. C* **80**, 044614 (2009).
 - [30] S. Rafi, M. Sharma, D. Pachouri, W. Haider, and Y. K. Gambhir, *Phys. Rev. C* **87**, 014003 (2013).
 - [31] B. S. Pudliner, V. R. Pandharipande, J. Carlson, S. C. Pieper, and R. B. Wiringa, *Phys. Rev. C* **56**, 1720 (1997).
 - [32] B. Friedman and V. R. Pandharipande, *Nucl. Phys. A* **361**, 502 (1981).
 - [33] I. E. Lagaris and V. R. Pandharipande, *Nucl. Phys. A* **359**, 349 (1981).
 - [34] R. B. Wiringa, V. G. J. Stoks, and R. Schiavilla, *Phys. Rev. C* **51**, 38 (1995).
 - [35] B. A. Loiseau, Y. Nogami, and C. K. Ross, *Nucl. Phys. A* **165**, 601 (1971).
 - [36] T. Kasahara, Y. Akaishi, and H. Tanaka, *Prog. Theor. Phys. Suppl.* **56**, 96 (1974).
 - [37] J. W. Holt, N. Kaiser, and W. Weise, *Phys. Rev. C* **81**, 024002 (2010).
 - [38] R. Machleidt, K. Holinde, and Ch. Elster, *Phys. Rep.* **149**, 1 (1987).
 - [39] K. Minomo, K. Ogata, M. Kohno, Y. R. Shimizu, and M. Yahiro, *J. Phys. G* **37**, 085011 (2010).
 - [40] M. Toyokawa, K. Minomo, and M. Yahiro, *Phys. Rev. C* **88**, 054602 (2013).
 - [41] B. Sinha, *Phys. Rep.* **20**, 1 (1975).
 - [42] B. Sinha and S. A. Moszkowski, *Phys. Lett. B* **81**, 289 (1979).
 - [43] G. R. Satchler and W. G. Love, *Phys. Rep.* **55**, 183 (1979).
 - [44] H. de Vries, C. W. de Jager, and C. de Vries, *At. Data Nucl. Data Tables* **36**, 495 (1987).
 - [45] R. P. Singhal, M. W. S. Macauley, and P. K. A. de Witt Huberts, *Nucl. Instr. and Meth.* **148**, 113 (1978).
 - [46] F. Nuoffer *et al.*, *Nuovo Cimento A* **111**, 971 (1998).
 - [47] M. Buenerd *et al.*, *Phys. Lett. B* **102**, 242 (1981).
 - [48] T. Furumoto and Y. Sakuragi, *Phys. Rev. C* **87**, 014618 (2013).
 - [49] M. Takechi *et al.*, *Phys. Rev. C* **79**, 061601(R) (2009).